Available online at www.sciencedirect.com
ScienceDirect
Phytochemistry 68 (2007) 2393–2404
PHYTOCHEMISTRY
www.elsevier.com/locate/phytochem

Dynamic flux cartography of hairy roots primary metabolism

M. Cloutier, M. Perrier, M. Jolicoeur *

Canada Research Chair on the Development of Metabolic Engineering Tools, Bio-P², Department of Chemical Engineering, Ecole Polytechnique de Montreal, P.O. Box 6079, Station Centre-ville, Montreal, Quebec, Canada H3C 3A7

Received 22 February 2007; received in revised form 16 April 2007
Available online 6 June 2007

Abstract

A dynamic model for plant cell and hairy root primary metabolism is presented. The model includes nutrient uptake (Pi, sugars, nitrogen sources), the glycolysis and pentose phosphate pathways, the TCA cycle, amino acid biosynthesis, respiratory chain, biosynthesis of cell building blocks (structural hexoses, organic acids, lipids, and organic phosphated molecules). The energy shuttles (ATP, ADP) and cofactors (NAD/H, NADP/H) are also included. The model describes the kinetics of 44 biochemical reactions (fluxes) of the primary metabolism of plant cells and includes 41 biochemical species (metabolites, nutrients, biomass components). Multiple Michaelis–Menten type kinetics are used to describe biochemical reaction rates. Known regulatory phenomena on metabolic pathways are included using sigmoid switch functions. A visualization framework showing fluxes and metabolite concentrations over time is presented. The visualization of fluxes and metabolites is used to analyze simulation results from *Catharanthus roseus* hairy root 50 d batch cultures. The visualization of the metabolic system allows analyzing split ratios between pathways and flux time-variations. For carbon metabolism, the cells were observed to have relatively high and stable fluxes for the central carbon metabolism and low and variable fluxes for anabolic pathways. For phosphate metabolism, a very high free intracellular Pi turnover rate was observed with higher flux variations than for the carbon metabolism. Nitrogen metabolism also exhibited large flux variations. The potential uses of the model are also discussed.

Keywords: Metabolic modelling; Hairy roots; Kinetic model; Metabolic regulation

1. Introduction

Plant metabolism has unique features that allow adaptation to a changing environment. Under Pi limitation, plant cells can activate pathways to bypass enzymatic reactions that require phosphate (Plaxton, 1998). Rontein et al. (2002) observed in tomato cells that the central primary metabolism fluxes are stable, but that the anabolic pathways (starch and other polysaccharide biosynthesis, amino and organic acid biosynthesis) can exhibit large variations, allowing the metabolism to adapt its behaviour to the cell's growth requirements. Gene expression in plant cells can also be correlated to intracellular ammonium concentration, as seen by Wong et al. (2004) in *Arabidopsis thaliana*. It is also well known that the intracellular concentrations in the nutrients and metabolites of plant cells can change significantly over time (Lamboursain and Jolicoeur, 2005). Thus, it is commonly accepted that plant cells have a complex metabolic capacity to adapt to a changing environment. An integrated approach in the analysis of plant cell metabolic pathways could thus yield important information on this metabolic capacity for adaptation. The most common method of accurately analyzing metabolic pathways and metabolic fluxes is the Metabolic Flux Analysis (MFA). However, since this method assumes a steady-state mass balance of metabolite concentrations, it can fail to grasp the dynamics of a metabolic system. The application of MFA to plant cell is still possible, as shown by Rontein et al. (2002), but it requires experimental conditions that can ensure the pseudo steady-state assumption.

A dynamic metabolic model was developed to account for the aforementioned specificities of plant cell metabolism

* Corresponding author. Tel.: +1 514 340 4711x4525; fax: +1 514 340 4159.
E-mail address: mario.jolicoeur@polymtl.ca (M. Jolicoeur).

0031-9422/$ - see front matter © 2007 Elsevier Ltd. All rights reserved.
doi:10.1016/j.phytochem.2007.04.028

(Leduc et al., 2006). This model describes metabolite and nutrient concentrations for *Catharanthus roseus* hairy roots in batch and medium exchange cultures. However, metabolite concentrations represent only the 'state' of a metabolic system, while the fluxes represent what the metabolism is 'performing'. The fluxes and turnover rates can be indicators of cell growth or biomolecule production potential. It was observed in mammalian cells that the ATP production rate is a good indicator of production potential (Lin et al., 1999; Henry et al., 2005). Thus, the description of metabolic fluxes with a dynamic model could potentially improve our capacity to understand and predict plant cell or hairy root biomolecule production potential. The central primary metabolism (glycolysis, TCA cycle, pentose-phosphate pathway, etc.) has been extensively studied, and many models can be found in the literature to analyze these pathways in bacterial cells and yeasts. The knowledge available on many organisms allows constructing reliable dynamic models that describe the kinetics of metabolic pathways. Chassagnole et al. (2002) proposed a dynamic model for the central carbon metabolism of *Escherichia coli* to study the influence of key enzymes on the global behaviour of the system. The dynamic modelling approach for the central carbon metabolism can also be applied to *Saccharomyces cerevisiae* fermentation, as seen by Rizzi et al. (1997). Metabolic models were also developed for plant cells. However, these models only described specific subnetworks like photosynthesis (Fridlyand and Scheibe, 1999; Poolman et al., 2000; Farquhar et al., 2001), respiration (Affourtit et al., 2001), cellulose biosynthesis (Delmer and Haigler, 2002), lipid biosynthesis (Ramli et al., 2002) or secondary metabolism (Boatright et al., 2004). Rontein et al. (2002) analyzed the central primary metabolism, but not dynamically. Thomas et al. (1997) studied the dynamics of potato tuber phosphofructokinase through Metabolic Control Analysis (MCA), but their work was limited to the dynamics of one enzyme. The model presented in Leduc et al. (2006) included the central primary metabolism, but with a steady-state hypothesis on metabolite concentrations. Thus, the fluxes and concentration profiles for the central metabolism were not described or analyzed. Moreover, the steady-state hypothesis limits the applicability of a metabolic model for plant cells, especially in a context where the high-throughput analytical methods allow the measurement of many parameters of a metabolic system. Metabolites can be measured by GC–MS (Roessner et al., 2000), fluxes can be estimated using isotope-labelled substrates (Dieuaide-Noubhani et al., 1995; Roscher et al., 2000), and gene expression can be measured with microarray analysis (Ruan et al., 1998). However, the amount of available information on metabolism is not yet sufficient to identify and understand all the metabolic regulation in plant cells. Therefore, the problems of dynamic metabolic modelling are still numerous. For instance, parameters identification is not trivial, even when a considerable dataset is available, and this can handicap the use of a model for prediction purposes. However, a fully dynamic metabolic model describing metabolite mass balances, enzyme kinetics, and pathway regulation can be a useful tool improving our capacity to analyze both hypotheses and experimental data on metabolic networks. To the best of our knowledge, no dynamic model for the central primary metabolism of plant cells can be found in the literature. In this work, we present a dynamic metabolic model for the primary metabolism of plant cells and show how the model can be used to obtain better insight into the metabolic behaviour of *C. roseus* hairy roots in batch culture. This dynamic metabolic modelling approach yields crucial information on a metabolic network since the resolution of such a system includes both concentration profiles and fluxes over time. Thus, a visualization framework that includes the fluxes and metabolite levels is proposed in analyzing the simulation results for the dynamic metabolic network.

2. Dynamic metabolic model for plant cells

2.1. General modelling approach

The dynamic metabolic model is based on the modelling approach presented in Leduc et al. (2006), but without the steady-state hypothesis on the primary metabolism. Thus, the model presented here fully describes the dynamics of the fluxes (44 reaction rates) and metabolite concentrations (41 biochemical species) of the metabolic network. The proposed metabolic network is presented in Fig. 1 and the stoichiometric equations are listed in Table 1. The metabolite mass balances of the system can be defined as an ensemble of ordinary differential equations (ODE) as follows:

$$\frac{dS}{dt} = M \cdot v - \mu \cdot S \tag{1}$$

where S is a vector of the 41 metabolite concentrations, M the stoichiometric matrix of the metabolic network, v the vector of the metabolic fluxes, and μ is the growth rate. This mathematical representation of a metabolic network is the most common one and there are several methods of solving it. The most common approach is the metabolic flux analysis (MFA). In that case a steady-state is assumed in metabolite concentrations, and the system can be solved by linear algebra since the left-hand side of Eq. (1) is equal to 0. However, the system is often underdetermined or it needs a set of known fluxes to be solved. This method is not necessarily well adapted for plant cell metabolism because plant cells are known to accumulate metabolites and nutrients, thus rendering the steady-state hypothesis dubious, except under certain conditions as discussed by Varner and Ramkrishna (1999). Rontein et al. (2002) also observed that the central carbon metabolism of tomato cells exhibits fluxes that are relatively high and stable, while the anabolic fluxes are lower and subject to

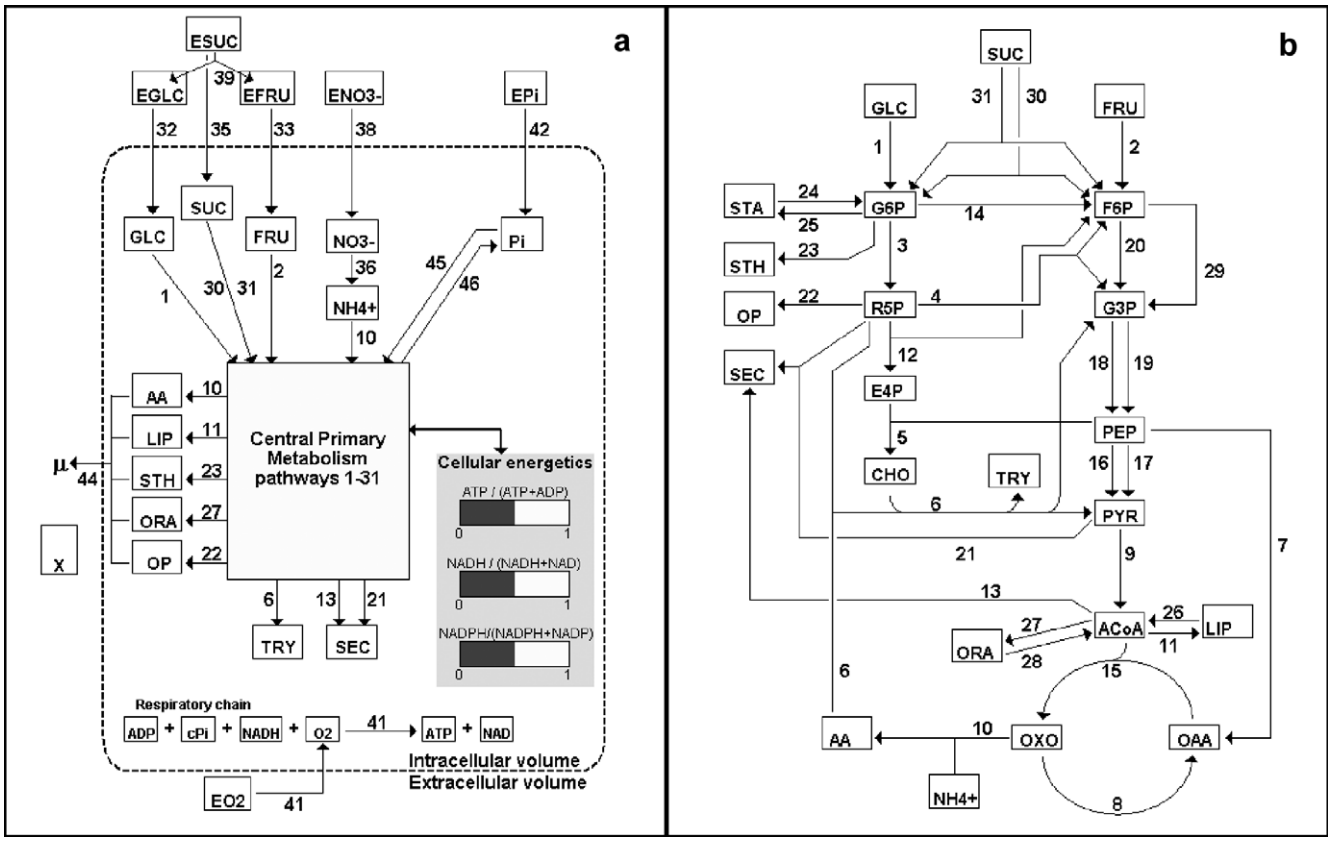

Fig. 1. Schematic view of the dynamic metabolic model (a) and pathways of the central primary metabolism (b). Numbers correspond to fluxes numbers in Tables 1–3.

variations. Thus, it is not altogether clear if a steady-state mass balance is the best way to analyze a plant cell metabolic system. It might be appropriate for a subset of reactions, as proposed in Leduc et al. (2006), but it still limits the analysis and the possible applications of a model. In this work, a fully kinetic metabolic model is presented. Each flux is described by a kinetic equation (Tables 2 and 3) of the form:

$$v(j) = v_{\max,j} \prod_i \frac{(S_i)^{\alpha_i}}{(K_{m,i})^{\alpha_i} + (S_i)^{\alpha_i}} \cdot f(S_i) \tag{2}$$

where each flux has a maximum reaction rate ($v_{\max,j}$), accounting for maximal potential active enzyme level. Then, each pathway regulation is described by multiplicative Michaelis–Menten type kinetics describing the effect of the substrates or cofactors and energy shuttles involved. The net global enzymatic activities are described macroscopically by lumping a series of effects. Thus, the model does not impose constant enzymatic activities. The main assumption here is that the driving forces behind the metabolic regulations are the variations in metabolites, co-factors and energy shuttles levels. This hypothesis showed to be efficient enabling the model to describe available data (see Section 3) but it remains a simplification which could be further developed. A single affinity constant ($K_{m,i}$) is used for each substrate. The exponent 'α_i' is used to represent higher reaction order. Moreover, sigmoid switch functions ($f(S_i)$, Eq. (3)) are multiplied by the reaction rates to describe known metabolic regulatory phenomena and maximum accumulation levels (see Tables 2 and 3). The general form of this function is:

$$f(S_i) = \frac{1}{1 + e^{-a(S_i - S_{i,t})}} \tag{3}$$

This function can switch from 0 to 1 around a threshold value ($S_{i,t}$) for a metabolite concentration. The parameter "a" defines the steepness of the regulation. This type of equation is more representative of biological behaviour than pure on/off switches. In a context of numerical solutions, it also reduces discontinuities around the threshold values. There are many functions that can describe sigmoid switches and the one proposed here was considered because of its simplicity (two parameters) and versatility in describing either sharp or smooth regulation (depending on the parameter "a").

This modelling approach requires the following parameter values for each individual reaction: $v_{\max}$, K_m and the regulation parameters "a" and $S_{i,t}$ when applicable. Initial conditions for the metabolite concentrations are also needed to solve the ODE problem. The advantage of this

Table 1
Reactions of the metabolic model

No.	Reaction
1	GLU + ATP → G6P + ADP
2	FRU + ATP → F6P + ADP
3	G6P + 2 NADP → R5P + 2 NADPH
4	3 R5P → 2 F6P + G3P
5	E4P + 2 PEP + ATP + NADH → CHO + 4 Pi + ADP + NAD
6	CHO + 2 AA + 2 ATP + R5P → PYR + 2 ADP + PPi + G3P + TRY
7	PEP + CO_2 → OAA + Pi
8	OXO+2 NAD + ADP + Pi → OAA + 2 NADH + ATP
9	PYR + NAD → NADH + ACOA
10	OXO + NH_4 + 3 NADPH + 3 ATP → AA + 3 NADP + 3 ADP + 3 Pi
11	ACOA + ATP + 2 NADPH → LIP + ADP + Pi + 2 NADP
12	2 R5P → F6P + E4P
13	3 ACOA + 2 NADPH + 3 ATP → SEC + 2 NADP + 3 ADP + 3 Pi
14	G6P → F6P
15	ACOA + OAA + NAD → OXO + NADH
16	PEP + ADP → PYR + ATP
17	PEP → PYR + Pi
18	G3P + Pi + ADP + NAD → PEP + ATP + NADH
19	G3P + NADP → PEP + NADPH
20	F6P + ATP → 2 G3P + ADP
21	R5P + PYR + ATP → SEC + ADP + 2 Pi
22	R5P + 3.75 AA + 7 ATP + 0.25 NAD → 7 ADP + 3.5 Pi + 1.75 PPi + 0.25 NADH + OP
23	G6P + 2 ATP + NADPH → STH + 2 ADP + NADP + Pi + PPi
24	STA + Pi → G6P
25	G6P + ATP → STA + ADP + PPi
26	LIP + 2 ATP + NAD → ACOA + 2 ADP + PPi + NADH
27	ACOA → ORA
28	ORA → ACOA
29	F6P + PPi → 2 G3P + Pi
30	SUC + 2 ATP → G6P + F6P + 2 ADP
31	SUC + PPi → G6P + F6P
32	EGLC + ATP → GLC + ADP + Pi
33	EFRU + ATP → FRU + ADP + Pi
34	OP → Pi
35	ESUC + ATP → SUC + ADP + Pi
36	NO_3 + NADH + 3 NADPH → NH_4 + NAD + 3 NADP
37	PPi → 2 Pi
38	ENO_3 + ATP → NO_3 + ADP + Pi
39	ESUC → EGLC + EFRU
40	ENH_4 + ATP → NH_4 + ADP + Pi
41	2.5 ADP + 2.5 Pi + NADH + O_2 → 2.5 ATP + NAD
42	EPi + 2 ATP → 3 Pi + 2 ADP
43	ATP → ADP + Pi
44	AA + LIP + ORA + STH + OP → X
45	$v8 + v18 + v24 + 2.5 * v41$
46	$4 * v5 + v7 + 3 * v10 + v11 + 3 * v13 + v17 + 2 * v21 + 3.5 * v22 + v23 + v29 + v33 + v34 + v35 + 2 * v37 + v38 + v40 + 3 * v41$

Table 2
Biokinetic equations and the regulation of metabolic fluxes 1–22

No.	Biokinetic equation
1	$v(1) = v_{\max 1} \cdot \frac{GLC}{K_{M_{GLC}}+GLC} \cdot \frac{ATP}{K_{M_{ATP}}+ATP}$
2	$v(2) = v_{\max 2} \cdot \frac{FRU}{K_{M_{FRU}}+FRU} \cdot \frac{ATP}{K_{M_{ATP}}+ATP}$
3	$v(3) = v_{\max 3} \cdot \frac{G6P}{K_{M_{G6P}}+G6P} \cdot \frac{NADP}{K_{M_{NADP}}+NADP} \cdot \frac{1}{1+e^{-10\cdot\left(\frac{NADP}{NADP+NADPH}-0.1\right)}}$
4	$v(4) = v_{\max 4} \cdot \frac{R5P}{K_{M_{R5P}}+R5P}$
5	$v(5) = v_{\max 5} \cdot \frac{E4P}{K_{M_{E4P}}+E4P} \cdot \frac{PEP}{K_{M_{PEP}}+PEP} \cdot \frac{ATP}{K_{M_{ATP}}+ATP} \cdot \frac{NADH}{K_{M_{NADH}}+NADH}$
6	$v(6) = v_{\max 6} \cdot \frac{CHO}{K_{M_{CHO}}+CHO} \cdot \frac{AA}{K_{M_{AA}}+AA} \cdot \frac{ATP}{K_{M_{ATP}}+ATP} \cdot \frac{R5P}{K_{M_{R5P}}+R5P}$
7	$v(7) = v_{\max 7} \cdot \frac{PEP}{K_{M_{PEP}}+PEP} \cdot \frac{CO_2}{K_{M_{CO2}}+CO_2}$
8	$v(8) = v_{\max 8} \cdot \frac{OXO}{K_{M_{OXO}}+OXO} \cdot \frac{NAD}{K_{M_{NAD}}+NAD} \cdot \frac{ADP}{K_{M_{ADP}}+ADP} \cdot \frac{Pi}{K_{M_{Pi}}+Pi}$
9	$v(9) = v_{\max 9} \cdot \frac{PYR}{K_{M_{PYR}}+PYR} \cdot \frac{NAD}{K_{M_{NAD}}+NAD}$
10	$v(10) = v_{\max 10} \cdot \frac{OXO}{K_{M_{OXO}}+OXO} \cdot \frac{NH_4}{K_{M_{NH4}}+NH_4} \cdot \frac{NADPH}{K_{M_{NADPH}}+NADPH} \cdot \frac{ATP}{K_{M_{ATP}}+ATP}$
11	$v(11) = v_{\max 11} \cdot \frac{ACOA}{K_{M_{ACOA}}+ACOA} \cdot \frac{ATP}{K_{M_{ATP}}+ATP} \cdot \frac{NADPH}{K_{M_{NADPH}}+NADPH}$
12	$v(12) = v_{\max 12} \cdot \frac{R5P}{K_{M_{R5P}}+R5P}$
13	$v(13) = v_{\max 13} \cdot \frac{ACOA}{K_{M_{ACOA}}+ACOA} \cdot \frac{NADPH}{K_{M_{NADPH}}+NADPH} \cdot \frac{ATP}{K_{M_{ATP}}+ATP}$
14	$v(14) = v_{\max 14} \cdot \frac{G6P}{K_{M_{G6P}}+G6P}$
15	$v(15) = v_{\max 15} \cdot \frac{ACOA}{K_{M_{ACOA}}+ACOA} \cdot \frac{OAA}{K_{M_{OAA}}+OAA} \cdot \frac{NAD}{K_{M_{NAD}}+NAD}$
16	$v(16) = v_{\max 16} \cdot \frac{PEP}{K_{M_{PEP}}+PEP} \cdot \frac{ADP}{K_{M_{ADP}}+ADP}$
17	$v(17) = v_{\max 17} \cdot \frac{PEP}{K_{M_{PEP}}+PEP} \cdot \left(1 - \frac{1}{1+e^{-10\cdot(Pi-1)}}\right)$
18	$v(18) = v_{\max 18} \cdot \frac{G3P}{K_{M_{G3P}}+G3P} \cdot \frac{Pi}{K_{M_{Pi}}+Pi} \cdot \frac{ADP}{K_{M_{ADP}}+ADP} \cdot \frac{NAD}{K_{M_{NAD}}+NAD}$
19	$v(19) = v_{\max 19} \cdot \frac{G3P}{K_{M_{G3P}}+G3P} \cdot \frac{NADP}{K_{M_{NADP}}+NADP}$
20	$v(20) = v_{\max 20} \cdot \frac{F6P}{K_{M_{F6P}}+F6P} \cdot \frac{ATP}{K_{M_{ATP}}+ATP}$
21	$v(21) = v_{\max 21} \cdot \frac{R5P}{K_{M_{R5P}}+R5P} \cdot \frac{PYR}{K_{M_{PYR}}+PYR} \cdot \frac{ATP}{K_{M_{ATP}}+ATP}$
22	$v(22) = v_{\max 22} \cdot \frac{R5P}{K_{M_{R5P}}+R5P} \cdot \frac{AA}{K_{M_{AA}}+AA} \cdot \frac{ATP}{K_{M_{ATP}}+ATP} \cdot \frac{NAD}{K_{M_{NAD}}+NAD} \cdot \frac{1}{1+e^{-32.7\cdot(Pi-0.0003)}}$

approach, where the dynamics of each reaction is described, is that the metabolic system is solved for both the fluxes and the metabolite concentrations. This allows for a complete description of the metabolic state of the system.

2.2. Nutrient uptake and accumulation

The major nutrients, i.e. glucose (GLC), fructose (FRU), sucrose (SUC), nitrate (NO_3), ammonium (NH_4) and phosphate (Pi), are taken up by the cell (respectively fluxes $v(32)$, $v(33)$, $v(35)$, $v(38)$, $v(40)$ and $v(42)$) and accumulated in intracellular pools (Fig. 1a). These pools then feed the reactions of the primary metabolism network.

2.3. Primary metabolism

The primary metabolism produces the cell building blocks: amino acids (AA), lipids (LIP), organic phosphates (OP, including nucleic acids), structural hexoses (STH),

Table 3
Biokinetic equations and the regulation of metabolic fluxes 23–45

No.	Biokinetic equation
23	$v(23) = v_{\max 23} \cdot \frac{G6P}{K_{M_{G6P}}+G6P} \cdot \frac{ATP}{K_{M_{ATP}}+ATP} \cdot \frac{NADPH}{K_{M_{NADPH}}+NADPH}$
24	$v(24) = v_{\max 24} \cdot \frac{STA}{K_{M_{STA}}+STA} \cdot \frac{Pi}{K_{M_{Pi}}+Pi} \cdot \left(1 - \frac{1}{1+e^{-100\cdot(GLC-0.2)}}\right)$
25	$v(25) = v_{\max 25} \cdot \frac{G6P}{K_{M_{G6P}}+G6P} \cdot \frac{ATP}{K_{M_{ATP}}+ATP} \cdot \frac{1}{1+e^{-10\cdot(GLC+FRU+SUC-0.2)}} \cdot \left(1 - \frac{1}{1+e^{-200\cdot(STA-1.7)}}\right)$
26	$v(26) = v_{\max 26} \cdot \frac{LIP}{K_{M_{LIP}}+LIP} \cdot \frac{ATP}{K_{M_{ATP}}+ATP} \cdot \frac{NAD}{K_{M_{NAD}}+NAD} \cdot \left(1 - \frac{1}{1+e^{-10\cdot(NADH-1)}}\right)$
27	$v(27) = v_{\max 27} \cdot \frac{ACOA}{K_{M_{ACOA}}+ACOA}$
28	$v(28) = v_{\max 28} \cdot \frac{ORA}{K_{M_{ORA}}+ORA} \cdot \left(1 - \frac{1}{1+e^{-10\cdot(NADH-1)}}\right)$
29	$v(29) = v_{\max 29} \cdot \frac{F6P}{K_{M_{F6P}}+F6P} \cdot \frac{PPi}{K_{M_{PPi}}+PPi} \cdot \left(1 - \frac{1}{1+e^{-10\cdot(Pi-1)}}\right)$
30	$v(30) = v_{\max 30} \cdot \frac{SUC}{K_{M_{SUC}}+SUC} \cdot \frac{ATP}{K_{M_{ATP}}+ATP} \cdot \left(1 - \frac{1}{1+e^{-100\cdot(GLC+FRU-0.02)}}\right)$
31	$v(31) = v_{\max 31} \cdot \frac{SUC}{K_{M_{SUC}}+SUC} \cdot \frac{PPi}{K_{M_{PPi}}+PPi}$
32	$v(32) = v_{\max 32} \cdot \frac{EGLC}{K_{M_{EGLC}}+EGLC} \cdot \frac{ATP}{K_{M_{ATP}}+ATP}$
33	$v(33) = v_{\max 33} \cdot \frac{EFRU}{K_{M_{EFRU}}+EFRU} \cdot \frac{ATP}{K_{M_{ATP}}+ATP}$
34	$v(34) = v_{\max 34} \cdot \frac{OP^4}{K^4_{M_{OP}}+OP^4} \cdot \left(1 - \frac{1}{1+e^{-15\cdot(Pi-0.045)}}\right)$
35	$v(35) = v_{\max 35} \cdot \frac{ESUC}{K_{M_{ESUC}}+ESUC} \cdot \frac{ATP}{K_{M_{ATP}}+ATP}$
36	$v(36) = v_{\max 36} \cdot \frac{NO_3^2}{K^2_{M_{NO3}}+NO_3^2} \cdot \frac{NADH}{K_{M_{NADH}}+NADH} \cdot \frac{NADPH}{K_{M_{NADPH}}+NADPH}$
37	$v(37) = v_{\max 37} \cdot \frac{PPi}{K_{M_{PPi}}+PPi}$
38	$v(38) = \left[v_{\max 38,LA} \cdot \frac{ENO_3}{K_{M,LA_{ENO3}}+ENO_3} + v_{\max 38,HA} \cdot \frac{ENO_3}{K_{M,HA_{ENO3}}+ENO_3}\right] \cdot \frac{ATP}{K_{M_{ATP}}+ATP}$
39	$v(39) = v_{\max 39} \cdot \frac{ESUC}{K_{M_{ESUC}}+ESUC}$
40	$v(40) = v_{\max 40} \cdot \frac{ATP}{K_{M_{ATP}}+ATP}$
41	$v(41) = v_{\max 41} \cdot \frac{NADH}{K_{M_{NADH}}+NADH} \cdot \frac{ADP}{K_{M_{ADP}}+ADP} \cdot \frac{Pi^2}{K^2_{M_{Pi}}+Pi^2} \cdot \frac{O_2}{K_{M_{O2}}+O_2}$
42	$v(42) = \left[v_{\max 42,LA} \cdot \frac{EPi}{K_{M,LA_{EPi}}+EPi} + v_{\max 42,HA} \cdot \frac{EPi}{K_{M,HA_{EPi}}+EPi}\right] \cdot \frac{ATP}{K_{M_{ATP}}+ATP}$
43	$v(43) = v_{\max 43} \frac{ATP}{K_{M_{ATP}}+ATP}$
44	$v(44) = v_{\max 44} \cdot X \cdot \frac{AA}{K_{M_{AA}}+AA} \cdot \frac{LIP^{1.25}}{K^{1.25}_{M_{LIP}}+LIP^{1.25}} \cdot \frac{ORA}{K_{M_{ORA}}+ORA} \cdot \frac{OP^4}{K^4_{M_{OP}}+OP^4}$

organic acids (ORA) as well as starch (STA). The primary metabolism reactions also include the balances on energy shuttles (ATP/ADP) and cofactors (NADH and NADPH, and their oxidized forms NAD and NADP). The major pathways of the central primary metabolism are included in the model, with simplifications in linear pathways. The model includes glycolysis (fluxes $v(1)$, $v(14)$, $v(16)$, $v(17)$, $v(18)$, $v(19)$, $v(20)$, $v(29)$) as well as pathways for the integration of other forms of sugars that are known to be used by plants: fructose (flux $v(2)$), sucrose (fluxes $v(30)$ and $v(31)$), and starch (flux $v(24)$). Some of the reactions (fluxes $v(16)$–$v(17)$, $v(18)$–$v(19)$ and $v(20)$–$v(29)$) are decoupled to account for phosphate regulation. Pyruvate (PYR) is channelled through secondary metabolite production (flux $v(21)$) or through the TCA cycle (fluxes $v(8)$, $v(9)$ and $v(15)$). Acetyl-Co-A (ACOA), apart from being consumed by the TCA cycle, is also the backbone in the production of organic acids (ORA, flux $v(27)$) and lipids (LIP, flux $v(11)$). These metabolic species are two of the cell's biomass 'building blocks' (X, reaction $v(44)$) and can also be degraded in ACOA (fluxes $v(26)$ and $v(28)$) under NADH limitation. The oxaloacetate (OAA) pool in the TCA cycle is replenished by the anaplerotic pathway ($v(7)$). Amino acid (AA) biosynthesis is included in a simplified pathway ($v(10)$) describing the fixation of NH_4 with oxoglutarate (OXO). Amino acids are used for growth ($v(44)$), as secondary metabolite precursors (tryptamine: TRY) biosynthesis ($v(6)$), or in organic phosphate (OP) biosynthesis ($v(22)$). The pentose phosphate pathway ($v(3)$, $v(4)$, $v(12)$) and the shikimate pathway ($v(5)$) are also described. Since many reactions of the primary metabolism either consume or release Pi, the turnover of this nutrient is illustrated by two 'global' fluxes: $v(45)$ and $v(46)$. Flux $v(45)$ is the sum of the fluxes that consume Pi and $v(46)$ is the sum of fluxes that release Pi. The model does not describe cell compartmentation and this may limit its biological significance for some specific fluxes which are taken as net fluxes. However, the structure of the model allows to include intracellular compartments when adequate experimental data are available for parameter calibration. Further explanations on the construction and regulation of the metabolic pathways and references for stoichiometric and kinetic parameters can be found in Leduc et al. (2006). Some of the parameters presented in Leduc et al. (2006) have changed because of the fully dynamic description of the central metabolism which implies that different metabolic interactions are described. However, many parameters did not change significantly between the two models.

2.4. Model calibration and determination of kinetic parameters

Model calibration was performed using experimental data from *C. roseus* hairy root cultures (Leduc et al., 2006). The data set is built with nutrient and metabolite measurements over time (45 d experiments). A complete description of the root line and culture conditions can be found in Leduc et al. (2006). The model simulations were done in Matlab (The Mathworks), using the ode15s.m subroutine for differential equations integration. The model has 40 affinity constants, 46 maximum reaction rates and

11 regulation functions with two parameters for a total of 108 parameters. These parameters were determined by error minimization between model predictions and experimental data using the lsqcurvefit.m subroutine. This subroutine is based on the Levenberg–Marquardt algorithm, which is appropriate for nonlinear curve-fitting. Initial estimates for the error minimization routine were taken from literature when available (see Leduc et al., 2006 for further details). The error minimization was performed using a set of 411 experimental data points. 14 state variables were measured (ENO_3, NO_3, NH_4, EPi, Pi, ESUC, SUC, EGLC, GLC, EFRU, FRU, AA, STA, X) in the two experiments (batch and medium exchange cultures). This data set is thus related to both medium nutrients and cell nutrition, cell amino acids and proteins pool (AA) and root mass (X). The model is over-parameterized, however, the use of values taken from the literature as initial estimates in the curve-fitting algorithm ensured to maintain the model parameters within a physiologically realistic range; i.e. between the lower and higher values found in literature. Parameters for the metabolic system are presented in Table 4 (affinity constants) and Table 5 (maximum reaction rates). Table 6 is a summary of the state variables of the system and initial conditions.

2.5. Visualization of primary metabolism

The full resolution of the metabolic model allows for the visualization of metabolic fluxes and metabolite concentrations. A visualization framework was thus established based on Fig. 1. This figure was built in the Matlab environment using the following graphical functions: line.m (for metabolic fluxes), patch.m (surface representation), text.m (add text to an image) and rectangle.m (for metabolites pools representation and graphical cell design). The simulated flux values, in mmol $gDW^{-1}\,d^{-1}$, are presented. The arrows thickness is changing proportionally to the fluxes numerical values. The metabolites simulated levels are also presented qualitatively, with a full square representing a high level for a metabolite and an empty square for a low level. The energetic state of the cell is also presented with graphical bar ranging from 0 to 1. The values in the graph for the energetic states are the following ratios: ATP/(ATP + ADP), NADH/(NADH + NAD), NADPH/(NADPH + NADP). Thus, a value of 0 represents a low energetic state, or a state in which the cofactors are in their oxidized form. A value near 1 represents a high energetic state, or a state with cofactors in their reduced form. For visualization purposes, the numerical solution of the system (fluxes and metabolites vectors) was sampled at a rate of five points per day over 50 d (251 points), thus producing 251 images. These 251 images were encoded at 10 frames per second using the Matlab functions getframe.m and movie2avi.m, thus producing a 25 s video representing the time course of the *C. roseus* batch culture. For clarity, the fluxes numerical values are updated only once per second. All the other elements of the visualization are updated frame by frame.

Table 4
Affinity constants (K_m)

Component	Value	Units
AA	0.045754	mmol gDW^{-1}
FRU	0.120	mmol gDW^{-1}
CO_2	1.25E−4	mmol gDW^{-1}
GLC	0.13844	mmol gDW^{-1}
LIP	0.00254	mmol gDW^{-1}
NAD	4.05E−4	mmol gDW^{-1}
NADH	4.492E−4	mmol gDW^{-1}
NADP	2E−4	mmol gDW^{-1}
NADPH	1.5E−4	mmol gDW^{-1}
ADP	1.1984E−4	mmol gDW^{-1}
NH_4	0.47157	mmol gDW^{-1}
ATP	0.00613	mmol gDW^{-1}
ORA	0.01	mmol gDW^{-1}
Pi	0.1006	mmol gDW^{-1}
PPi	2.43E−4	mmol gDW^{-1}
SUC	1.00	mmol gDW^{-1}
STA	1.00	mmol gDW^{-1}
STH	0.248	mmol gDW^{-1}
OP	0.003994	mmol gDW^{-1}
G6P	0.0126	mmol gDW^{-1}
F6P	0.0113	mmol gDW^{-1}
G3P	0.0149	mmol gDW^{-1}
E4P	0.0127	mmol gDW^{-1}
R5P	0.0177	mmol gDW^{-1}
CHO	0.0124	mmol gDW^{-1}
PYR	0.0132	mmol gDW^{-1}
PEP	0.0123	mmol gDW^{-1}
ACOA	0.0125	mmol gDW^{-1}
OAA	0.0122	mmol gDW^{-1}
OXO	0.0131	mmol gDW^{-1}
O_2	5.75E−5	mmol gDW^{-1}
NO_3	0.2007	mmol gDW^{-1}
EFRU	0.0461	mM
EGLC	0.0535	mM
ENO_3_HA	0.0677	mM
ENO_3_LA	0.4317	mM
EPI_HA	0.0026	mM
EPI_LA	0.050	mM
ESUC	12.012	mM
EO_2	0.0125	mM

3. Results and discussion

3.1. The model describes hairy roots growth and metabolic behaviour

The model presented here without the steady-state hypothesis on the central primary metabolism described adequately the cellular behaviour, with respect to the available data for a batch culture of *C. roseus* (Fig. 2) [data from Leduc et al. (2006)]. The medium exchange culture experimental data was also simulated (results not shown). The model is thus able to describe the uptake of carbohydrates, nitrate and phosphate, and their respective intracellular accumulation in specific pools (i.e. chemically

Table 5
Maximum reaction rates (V_{max})

Reaction	Current value	Units
1	2.4938	mmol gDW^{-1} d^{-1}
2	5.2712	mmol gDW^{-1} d^{-1}
3	1.3658	mmol gDW^{-1} d^{-1}
4	0.0047	mmol gDW^{-1} d^{-1}
5	9.8429	mmol gDW^{-1} d^{-1}
6	2.4765	mmol gDW^{-1} d^{-1}
7	2.9044	mmol gDW^{-1} d^{-1}
8	195.17	mmol gDW^{-1} d^{-1}
9	47.114	mmol gDW^{-1} d^{-1}
10	2.5266	mmol gDW^{-1} d^{-1}
11	0.8043	mmol gDW^{-1} d^{-1}
12	0.1214	mmol gDW^{-1} d^{-1}
13	0.2722	mmol gDW^{-1} d^{-1}
14	0.544	mmol gDW^{-1} d^{-1}
15	60.369	mmol gDW^{-1} d^{-1}
16	11.891	mmol gDW^{-1} d^{-1}
17	1.1416	mmol gDW^{-1} d^{-1}
18	135.94	mmol gDW^{-1} d^{-1}
19	9.0472	mmol gDW^{-1} d^{-1}
20	17.891	mmol gDW^{-1} d^{-1}
21	0.0199	mmol gDW^{-1} d^{-1}
22	3.6042	mmol gDW^{-1} d^{-1}
23	0.0783	mmol gDW^{-1} d^{-1}
24	0.0022	mmol gDW^{-1} d^{-1}
25	0.424	mmol gDW^{-1} d^{-1}
26	0.008	mmol gDW^{-1} d^{-1}
27	0.0682	mmol gDW^{-1} d^{-1}
28	0.0001	mmol gDW^{-1} d^{-1}
29	1.5167	mmol gDW^{-1} d^{-1}
30	0.01	mmol gDW^{-1} d^{-1}
31	0.1232	mmol gDW^{-1} d^{-1}
32	1.175	mmol gDW^{-1} d^{-1}
33	0.929	mmol gDW^{-1} d^{-1}
34	0.0096	mmol gDW^{-1} d^{-1}
35	0.05	mmol gDW^{-1} d^{-1}
36	0.3688	mmol gDW^{-1} d^{-1}
37	2.9016	mmol gDW^{-1} d^{-1}
38 HA	0.0015	mmol gDW^{-1} d^{-1}
38 LA	0.2868	mmol gDW^{-1} d^{-1}
39	1.002	mmol gDW^{-1} d^{-1}
40	0	mmol gDW^{-1} d^{-1}
41	13.2	mmol gDW^{-1} d^{-1}
42 HA	0.00175	mmol gDW^{-1} d^{-1}
42 LA	0.1101	mmol gDW^{-1} d^{-1}
43	1.132	mmol gDW^{-1} d^{-1}
44	0.15	d^{-1}
45	–	–
46	–	–

Table 6
State variables and initial conditions

Component	Value	Units
AA	0.818	mmol gDW^{-1}
FRU	0.0336	mmol gDW^{-1}
CO_2	1.25E−3	mmol gDW^{-1}
GLC	0.1625	mmol gDW^{-1}
SEC	0.00515	mmol gDW^{-1}
TRY	8.722E−4	mmol gDW^{-1}
LIP	0.1	mmol gDW^{-1}
NAD	5.9E−5	mmol gDW^{-1}
NADH	2E−4	mmol gDW^{-1}
NADP	1.8E−5	mmol gDW^{-1}
NADPH	1.45E−4	mmol gDW^{-1}
ADP	7.13E−4	mmol gDW^{-1}
NH_4	0.053	mmol gDW^{-1}
ATP	1.296E−3	mmol gDW^{-1}
ORA	0.00807	mmol gDW^{-1}
Pi	0.117	mmol gDW^{-1}
PPi	3.5E−5	mmol gDW^{-1}
SUC	0.403	mmol gDW^{-1}
STA	1.705	mmol gDW^{-1}
STH	0.01	mmol gDW^{-1}
OP	6.7E−3	mmol gDW^{-1}
G6P	0.0125	mmol gDW^{-1}
F6P	0.0122	mmol gDW^{-1}
G3P	0.0131	mmol gDW^{-1}
E4P	0.0127	mmol gDW^{-1}
R5P	0.0126	mmol gDW^{-1}
CHO	0.0119	mmol gDW^{-1}
PYR	0.0130	mmol gDW^{-1}
PEP	0.0125	mmol gDW^{-1}
ACOA	0.0124	mmol gDW^{-1}
OAA	0.0126	mmol gDW^{-1}
OXO	0.0121	mmol gDW^{-1}
O_2	1.15E−3	mmol gDW^{-1}
NO_3	0.385	mmol gDW^{-1}
EFRU	8.33	mM
EGLC	7.22	mM
ENO_3	3.27	mM
ENH_4	0	mM
EPI	0.1	mM
ESUC	114	mM
EO_2	0. 25	mM

compartmented but not into organelles). Moreover, the cell behaviour (in this case cell growth) is also described. Thus, the fluxes and the metabolites levels, although not yet experimentally identified, are within a physiological range since the 'extremities' of the model (input to the cell and cell behaviour) are well described (see also Leduc et al. (2006) for exhaustive comparison with literature). The rates of nutrients transport (Table 3, fluxes 32, 33, 38, 39 and 42) are mediated by the ATP level in the cell (i.e. ATPases for pH regulation), thus including an indicator of the cell physiological state in the description of nutrients uptake. So the model accounts for physiological variations that could affect enzymes activities and, in the case of nutrient transport, this strategy seems to be reliable enough to describe the experimental data.

3.2. Metabolic flux cartography to visualize metabolic networks

Flux cartography is presented in Figs. 3 and 4. Fig. 3a presents the metabolic system after 5 d of a batch culture, with the hairy roots in early exponential phase. Fig. 3b presents the system after 15 d, when the roots are in exponential growth. Fig. 4a presents the deceleration phase (35 d). Finally, Fig. 4b presents the metabolic state of the hairy roots at the end of a batch culture (50 d), when the roots are in stationary phase. This complete visualization of the metabolic system over time is discussed in the following sections. The 25 s video of the simulation of the dynamic

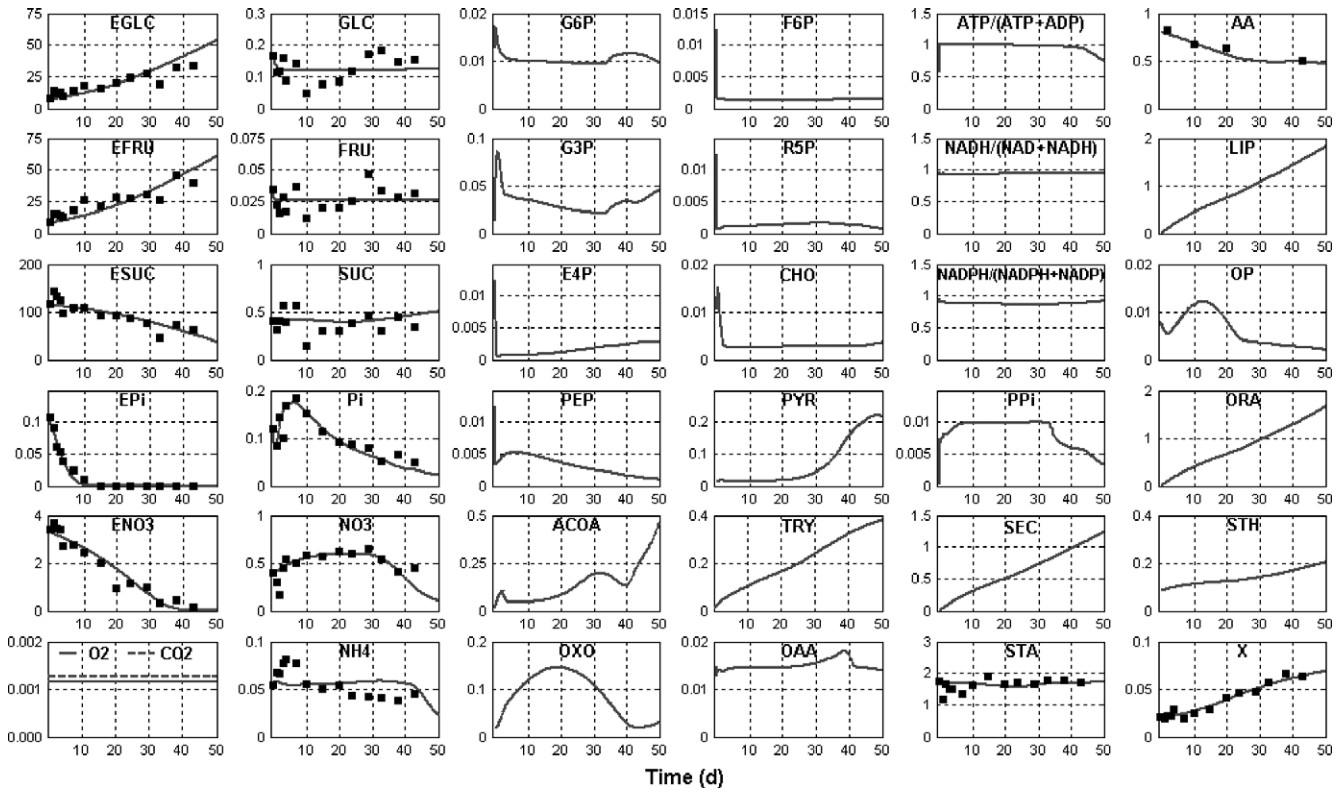

Fig. 2. Simulated metabolites profiles and experimental data for a batch culture of *C. roseus*. Axis units are mmol gDW^{-1} except for X (gDW Petri $dish^{-1}$) and for extracellular nutrients EGLC, EFRU, ESUC, EPi, ENO_3 (mmol).

metabolic system is also provided. Figs. 3 and 4 are snapshots taken from that video.

3.3. Carbon metabolism

Flux distribution shows that the entering fluxes of carbon sources to the primary metabolism ($v(1)$ and $v(2)$) are relatively high, even at the beginning of the exponential growth phase (Fig. 3a). These fluxes are also stable through the culture phases. A decrease of 15% is observed only at the end of the batch culture. This decrease is attributed to a lower energetic state of the roots (see Fig. 4b, 'cellular energetics') since the intracellular pools in GLC and FRU were still at a high level. The first steps of glycolysis ($v(14)$ and $v(20)$) were also stable, showing a decrease of 3.6% and 11.5%, respectively. The next step in glycolysis, the conversion of G3P to PEP, can be performed by two different pathways in the model: $v(18)$ and $v(19)$. Flux $v(19)$ exhibited a decrease of 17% due to a combined decrease in G3P and NADP concentrations. Flux $v(18)$ was stable through the culture time with observed variations of only 3%. The conversion of PEP to PYR shows larger variations in fluxes. Flux $v(16)$ increased from 0.59 mmol $gDW^{-1}\,d^{-1}$ to a maximum of 0.88 mmol $gDW^{-1}\,d^{-1}$ at 35 d and a final value of 0.81 mmol $gDW^{-1}\,d^{-1}$. At the same time, flux $v(17)$ decreased from 0.34 mmol $gDW^{-1}\,d^{-1}$ at 5 d to a final value of 0.08 mmol $gDW^{-1}\,d^{-1}$. Thus, the global flux from PEP to PYR is relatively stable, with a decrease of only 4.3% over 50 d. This allows maintaining the flux to PYR even though the metabolic state of the system is changing. The flux distribution in Figs. 3 and 4 shows that most of the ACOA coming from flux $v(9)$ is channelled through the TCA cycle (fluxes $v(8)$ and $v(15)$). At the beginning of the culture, flux $v(15)$ is equal to 75% of flux $v(9)$, while at the end this proportion is 65%. The ACOA that is not channelled through the TCA cycle is either accumulated or feeds the anabolic pathways $v(11)$ and $v(27)$ to produce LIP and ORA. At the beginning of the exponential phase (Fig. 3a), 5.1% of flux $v(9)$ is channelled to ORA and 9.5% to LIP. These proportions are, respectively, 7% and 10.5% at the end of the batch culture (Fig. 4b). The other pathways related to carbon metabolism, the pentose phosphate pathway, and the shikimate pathway, showed much lower fluxes, ranging from 2.7×10^{-4} to 4.4×10^{-2} mmol $gDW^{-1}\,d^{-1}$. These fluxes exhibited larger variations over time in the range of 25–30%. The biosynthesis of STA and STH was also channelling only a fraction of the glycolytic flux throughout the culture. The STH production flux $v(23)$ was equal to 1.6% of the entering glucose metabolic flux ($v(1)$). The flux for starch accumulation ($v(25)$) was equal to 14% of $v(1)$ at the beginning of the exponential phase, 15.5% when the growth rate was at its maximum value (Fig. 3b), and this proportion decreased to 4% at the end of the batch experiment (Fig. 4b). However, this decrease was not caused by a limitation in G6P, but rather by a lower energetic state at the

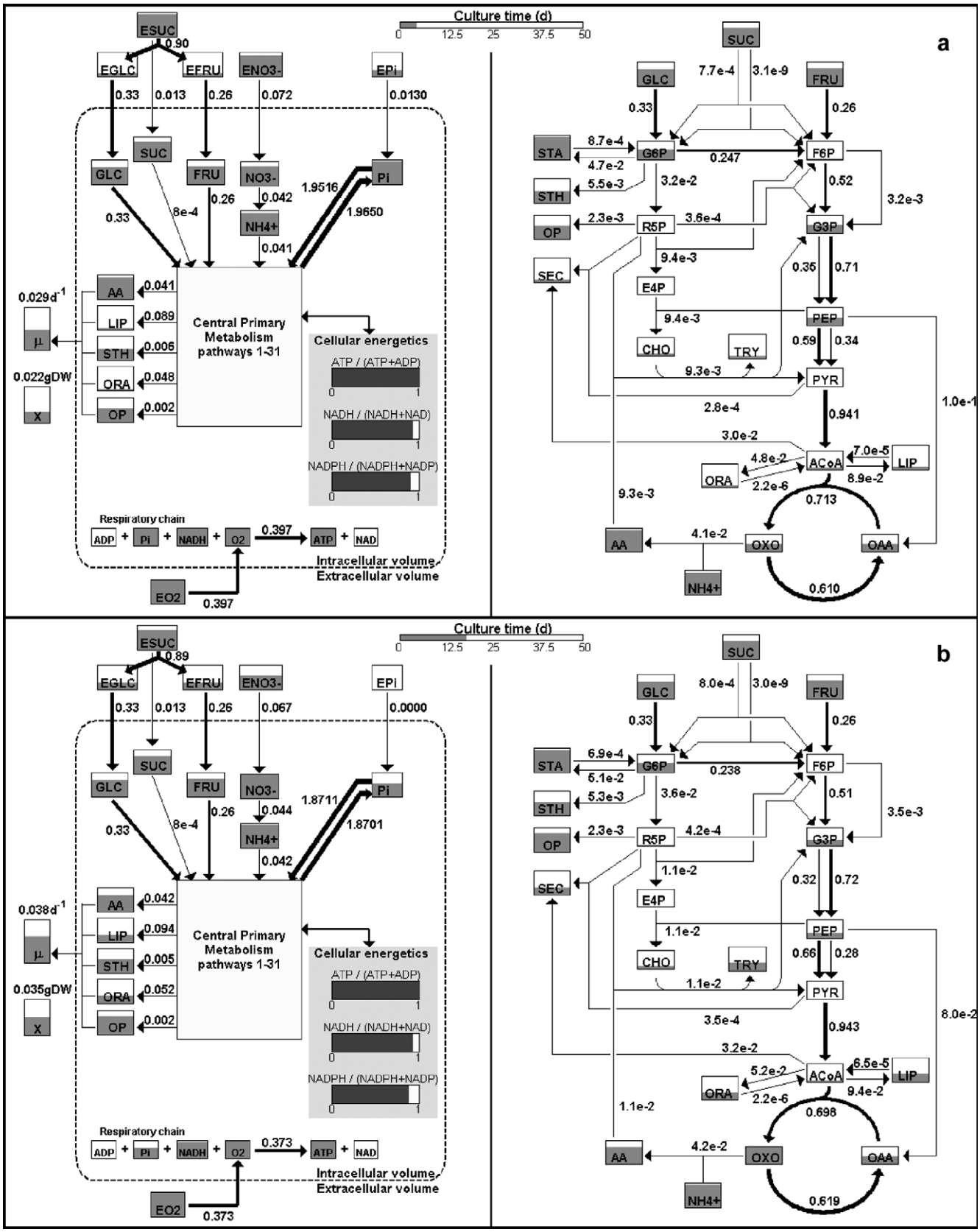

Fig. 3. Cartography of simulated fluxes for a batch culture. Early exponential phase after 5 d (a). Exponential growth phase after 15 d (b). Fluxes units are mmol $gDW^{-1}\,d^{-1}$.

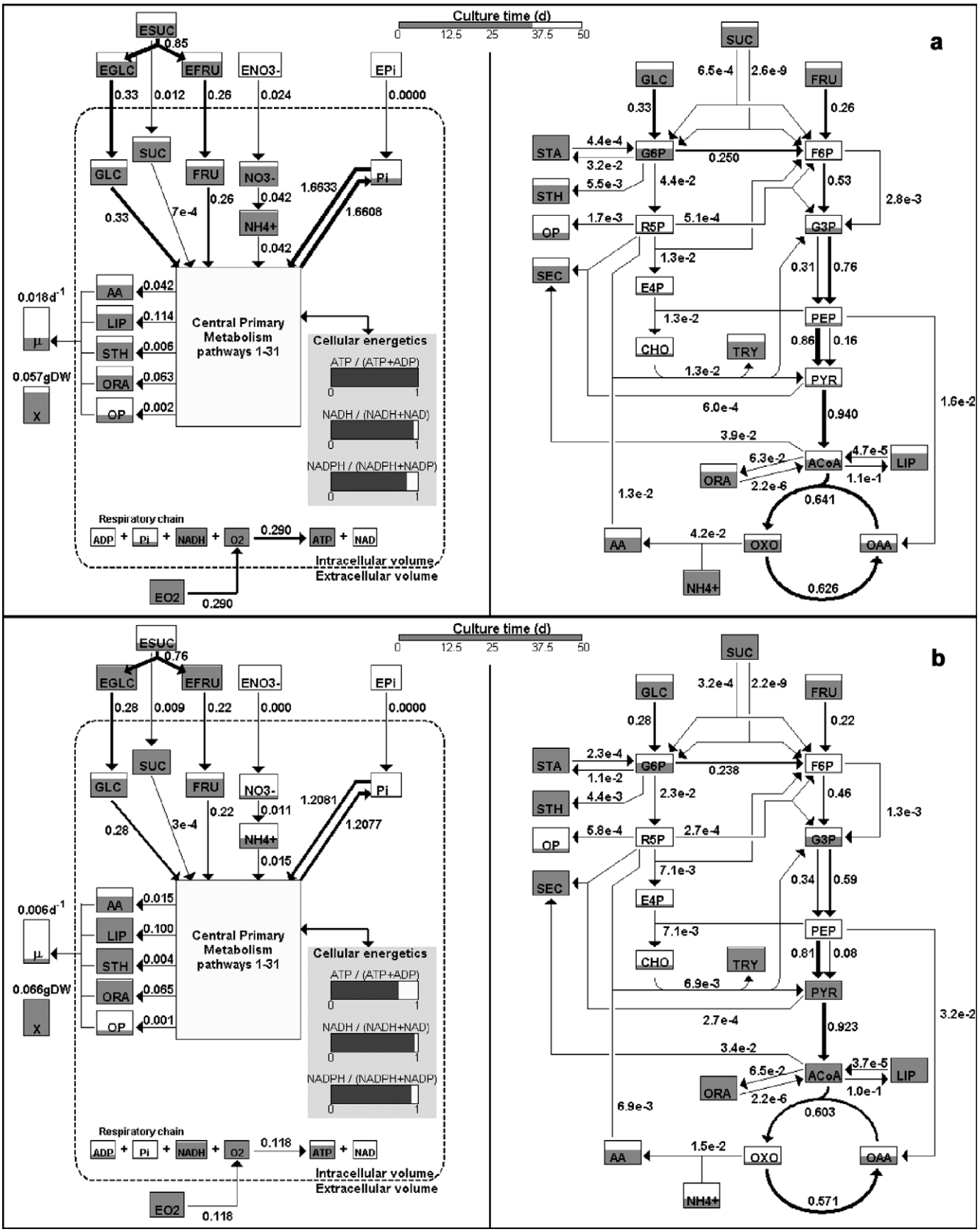

Fig. 4. Cartography of simulated fluxes for a batch culture. Deceleration phase after 35 d (a). Stationary phase after 50 d (b). Fluxes units are mmol gDW^{-1} d^{-1}.

end of the growth phase. Thus, it seems that a high and relatively stable flux in the central carbon metabolism is observed even in the case where the cells are not in growth phase. Analysis of simulation results suggests that energetic metabolism might have a greater impact on the anabolic fluxes than the availability of carbon backbones. This strategy allows maintaining stability in the central primary metabolism, while the anabolic pathways have higher flexibility (as seen by Rontein et al., 2002). It is also noteworthy to mention that no carbohydrate limitation was observed in that experiment (Leduc et al., 2006). Glucose and fructose were still present in the culture medium and in the hairy root intracellular pools at the end of the batch culture, as can be seen in Fig. 4b.

3.4. Phosphate and energetic metabolism

The fluxes related to phosphate metabolism exhibited higher variations than those related to carbon. The entering flux of Pi in the cell ($v(42)$) went from an initial value of 0.02 mmol gDW^{-1} d^{-1} to complete exhaustion of the Pi in the culture medium after 10 d, thus a null uptake flux for Pi. However, this exhaustion of Pi in the culture medium will not lead to an immediate limitation in Pi since the intracellular Pi pool can supply the Pi-consuming reactions. The biosynthesis of organic phosphates (OP, $v(22)$) decreased from 2.3×10^{-3} mmol gDW^{-1} d^{-1} at the beginning of the experiment to 5.8×10^{-4} mmol gDW^{-1} d^{-1} at the end. This 75% decrease is attributed to a less energetic state and a lower level in cellular Pi, which affect the regulation in $v(22)$ (see Table 2). The global fluxes for Pi consumption or release by the primary metabolism are very high compared to the other simulated fluxes. At the beginning of the batch culture (Fig. 3a), $v(45)$ and $v(46)$ are both more than two times higher than the third highest flux, $v(39)$. Since the intracellular concentration in Pi decreases over time, most of the reactions using Pi slow down. Thus, the influx of Pi to metabolism ($v(45)$) exhibits a decrease of 35% compared to its initial value. The release of Pi by the central metabolism exhibits the same behaviour. The fluxes $v(45)$ and $v(46)$ are also two to three orders of magnitude higher than the net influx of Pi to metabolism ($v(45)$–$v(46)$). Thus, a high 'turnover' rate of Pi is observed. This turnover rate could be an interesting physiological indicator of the cellular activity or cell potential for growth or biomolecules production. However, it is hard to confirm this hypothesis comparing to literature results since most of the works on the turnover of phosphate are focussing on the turnover rate of one key enzyme or one phosphated molecule. Alonso et al. (2005) observed a glucose-P-to-glucose turnover in maize root tips. This cycle showed to consume 40% of the generated ATP and was affected by carbohydrate starvation. The respiratory chain ($v(41)$) shows a continuous decrease from an initial rate of 0.397 mmol gDW^{-1} d^{-1} to 0.118 mmol gDW^{-1} d^{-1}. This 70% decrease is due to the decreasing level of Pi and roughly corresponds to the 75% decrease observed for the biosynthesis of OP. The global modelling approach thus shows how a nutrient could limit more than one pathway at a time. Here Pi seems to be affecting the respiratory chain and reactions of the central carbon metabolism.

3.5. Nitrogen metabolism

The extracellular nitrogen source (NO_3), like the phosphate source, was depleted during the culture time period. Thus, the entering flux of NO_3 in the cells falls to zero at the end of the culture from an initial value of 0.072 mmol gDW^{-1} d^{-1}. This triggers a decrease in the intracellular nitrate pool, and subsequently in the intracellular ammonium pool (Fig. 4). The fluxes connected to these pools ($v(10)$ and $v(36)$) decreased by a 75% at the end of the simulation. However, this occurs only after 35 d (Fig. 4a), when the growth rate is already decreasing. The decrease in growth rate and in many fluxes is then not directly related to a nitrogen limitation. Amino acids were still present at a relatively high level at the end of the culture (Fig. 4b), even though the rate of production decreased. Thus, it is more likely that the medium used in these experiments limited the cells in Pi. However, the fluxes related to nitrogen also exhibited a decrease after 35 d of culture, so a limitation could occur for that nutrient as well.

4. Conclusion

A comprehensive dynamic metabolic model was presented. The model describes the major pathways of plant cell primary metabolism. The strategy used to solve the metabolic system involves the description of the kinetics of each enzymatic reaction. Multiple Michaelis–Menten type kinetics, in conjunction with sigmoid switch functions, allows describing the dynamic behaviour of the metabolic system subject to diverse regulatory phenomena. In order to better analyze the simulation results, a visualization framework including both the fluxes and metabolite levels was presented. It was observed that the central carbon metabolism had relatively high and stable fluxes, while most of the anabolic pathways had small and variable fluxes. The nitrogen metabolism exhibited considerable variations in the fluxes, but the amino acids pool was still at a high level at the end of the culture. However, it was observed that phosphate and phosphate-related pathways play a crucial role on cell behaviour. Reactions from the glycolysis, respiration, and energy metabolism were probably affected by a Pi limitation. Moreover, it was observed that the intracellular Pi is subject to a 'turnover' rate that is two to three orders of magnitude higher than the actual Pi consumed by the primary metabolism reactions. This turnover of Pi decreased in conjunction with a decrease in intracellular Pi. A decrease in specific growth rate also occurred in conjunction with the Pi decrease. Thus, it is

seen that Pi is a crucial element in explaining plant cell behaviour, not only in terms of the growth rate but also by considering metabolic processes such as glycolysis, respiration etc. The dynamic approach thus shows useful in identifying important dynamic phenomena that explain plant cell behaviour. It is clear that this model can be improved with further analyses (metabolites levels, enzymatic and compartment analyses) and experiments that are specifically designed for parameters identification such as perturbations and step-response experiments. This procedure could certainly improve the reliability of the parameters and the predictive capacity of the model. Moreover, the metabolic model presented in this work could be used in conjunction with proper analytical methods (measurement of metabolites concentrations, enzymatic activity, gene expression) to integrate knowledge on plant cell metabolism. A reliable dynamic model could also be used to identify potential targets for metabolic engineering or to develop efficient culture strategies.

Appendix A. Supplementary data

Supplementary data associated with this article can be found, in the online version, at doi:10.1016/j.phytochem.2007.04.028.

References

Affourtit, C., Krab, K., Moore, A.L., 2001. Control of plant mitochondrial respiration. Biochimica et Biophysica Acta (BBA) – Bioenergetics 1504, 58–69.

Alonso, A.P., Vigeolas, H., Raymond, P., Rolin, D., Dieuaide-Noubhani, M., 2005. A new substrate cycle in plants. Evidence for a high glucose-phosphate-to-glucose turnover from in vivo steady-state and pulse-labeling experiments with [^{13}C]glucose and [^{14}C]glucose. Plant Physiology 138, 2220–2232.

Boatright, J., Negre, F., Chen, X., Kish, C.M., Wood, B., Peel, G., Orlova, I., Gang, D., Rhodes, D., Dudareva, N., 2004. Understanding in vivo benzenoid metabolism in petunia petal tissue. Plant Physiology 135, 1993–2011.

Chassagnole, C., Noisommit-Rizzi, N., Schmid, J.W., Mauch, K., Reuss, M., 2002. Dynamic modeling of the central carbon metabolism of *Escherichia coli*. Biotechnology and Bioengineering 79, 53–73.

Delmer, D.P., Haigler, C.H., 2002. The Regulation of Metabolic Flux to Cellulose, a Major Sink for Carbon in Plants. Metabolic Engineering 4, 22–28.

Dieuaide-Noubhani, M., Raffard, G., Canioni, P., Pradet, A., Raymond, P., 1995. Quantification of compartmented metabolic fluxes in maize root tips using isotope distribution from ^{13}C- or ^{14}C-labeled glucose. The Journal of Biological Chemistry 270, 13147–13159.

Farquhar, G.D., von Caemmerer, S., Berry, J.A., 2001. Models of Photosynthesis. Plant Physiology 125, 42–45.

Fridlyand, L.E., Scheibe, R., 1999. Regulation of the Calvin cycle for CO_2 fixation as an example for general control mechanisms in metabolic cycles. Biosystems 51, 79–93.

Henry, O., Perrier, M., Kamen, A., 2005. Metabolic flux analysis of HEK-293 cells in perfusion cultures for the production of adenoviral vectors. Metabolic Engineering 7, 467–476.

Lamboursain, L., Jolicoeur, M., 2005. Critical influence of Eschscholzia californica cells nutritional state on secondary metabolite production. Biotechnology and Bioengineering 91, 827–837.

Leduc, M., Tikhomiroff, C., Cloutier, M., Perrier, M., Jolicoeur, M., 2006. Development of a kinetic metabolic model: application to *Catharanthus roseus* hairy root. Bioprocess and Biosystems Engineering 28, 295–313.

Lin, J., Takagi, M., Qu, Y., Gao, P., Yoshida, T., 1999. Metabolic flux change in hybridoma cells under high osmotic pressure. Journal of Bioscience and Bioengineering 87, 255–257.

Plaxton, W.C., 1998. Metabolic aspects of phosphate starvation in plants. In: Lynch, J.P., Deikman, J. (Eds.), Phosphorus in Plant Biology: Regulatory Roles in Molecular, Cellular, Organismic, and Ecosystem Processes. American Society of Plant Physiologists, pp. 229–241.

Poolman, M.G., Fell, D.A., Thomas, S., 2000. Modelling photosynthesis and its control. Journal of Experimental Botany 51, 319–328.

Ramli, U.S., Baker, D.S., Quant, P.A., Harwood, J.L., 2002. Control analysis of lipid biosynthesis in tissue cultures from oil crops shows that flux control is shared between fatty acid synthesis and lipid assembly. Biochemical Journal 364, 393–401.

Rizzi, M., Baltes, M., Theobald, U., Reuss, M., 1997. In vivo analysis of metabolic dynamics in *Saccharomyces cerevisiae*: II. Mathematical model. Biotechnology and Bioengineering 55, 592–608.

Roessner, U., Wagner, C., Kopka, J., Trethewey, R.N., Willmitzer, L., 2000. Simultaneous analysis of metabolites in potato tuber by gas chromatography–mass spectrometry. Plant Journal 23, 131–142.

Rontein, D., Dieuaide-Noubhani, M., Dufourc, E.J., Raymond, P., Rolin, D., 2002. The metabolic architecture of plant cells: stability of central metabolism and flexibility of anabolic pathways during the growth cycle of tomato cells. Journal of Biological Chemistry 277, 43948–43960.

Roscher, A., Kruger, N.J., Ratcliffe, R.G., 2000. Strategies for metabolic flux analysis in plants using isotope labelling. Journal of Biotechnology 77, 81–102.

Ruan, Y., Gilmore, J., Conner, T., 1998. Towards Arabidopsis genome analysis: monitoring expression profiles of 1400 genes using cDNA microarrays. Plant Journal 15, 821–833.

Thomas, S., Mooney, P.J., Burrell, M.M., Fell, D.A., 1997. Metabolic Control Analysis of glycolysis in tuber tissue of potato (Solanum tuberosum): explanation for the low control coefficient of phosphofructokinase over respiratory flux. Biochemical Journal 322, 119–127.

Varner, J., Ramkrishna, D., 1999. Mathematical models of metabolic pathways. Current Opinion in Biotechnology 10, 146–150.

Wong, H.-K., Chan, H.-K., Coruzzi, G.M., Lam, H.-M., 2004. Correlation of ASN2 gene expression with ammonium metabolism in Arabidopsis. Plant Physiology 134, 332–338.